EUROFUSION WPMST1-PR(16) 15910

G Cseh et al.

Pellet cloud characterisation, scaling and estimation of the material- and temperature distribution inside the cloud

Preprint of Paper to be submitted for publication in
Nuclear Fusion

This work has been carried out within the framework of the EUROfusion Consortium and has received funding from the Euratom research and training programme 2014-2018 under grant agreement No 633053. The views and opinions expressed herein do not necessarily reflect those of the European Commission.

Pellet cloud characterisation, scaling and estimation of the material- and temperature distribution inside the cloud

G. Cseh, G. Kocsis, P. T. Lang, B. Plöckl, T. Szepesi, G. Veres
and the ASDEX Upgrade Team

19th May 2016

Abstract

Using spatially calibrated images of fast visible cameras, a database was established containing pellet cloud images and the related pellet- and plasma parameters. Using this database, two scalings were derived for the cloud length along the magnetic field lines as a function of pellet speed and ablation rate (first case) and pellet speed, pellet volume, plasma temperature and plasma density (second case). Using the images - based on the number of radiation maxima - the four main cloud shapes were also categorized. The isotope effect (the effect of hydrogen pellets in hydrogen or helium plasma) was also investigated with particular attention devoted to the cloud characteristics. Finally, a synthetic diagnostic - which simulates the measurement system and produces a synthetic pellet cloud image based on the output of pellet cloud simulations - was developed to reveal the underlying density- and temperature distributions of the observed pellet cloud images. Using this synthetic diagnostic, one of the main identified cloud shapes was reconstructed. Our goal is to derive a scaling law for the toroidal extension of the pellet cloud at different pellet- and plasma conditions, to give a more reliable input for the pellet ELM triggering simulations and using these two results - a better understanding of the pellet-caused pressure perturbation.

1 Introduction

Cryogenic pellet injection is one of the most promising methods to efficiently fuel fusion plasmas[1, 2]. To optimise fuelling efficiency, it is important to determine, how

deep the pellet penetrated into the plasma, before the material has fully ablated (pellet penetration depth), how this material is deposited along the pellet path (deposition profile), and how these two quantities depend on the different pellet- and plasma parameters. Experimental scaling at Axially Symmetric Divertor EXperiment (ASDEX) Upgrade (AUG) tokamak for H-mode plasmas on High Field Side (HFS) pellet injection[3] shows, that the main parameters determining the pellet penetration depth are the pellet speed, size, plazma density and temperature and the applied magnetic field[4]. These findings are in fair agreement (despite the lack of magnetic field effect) with the results of the hybrid pellet simulation code (combination of the LLP [5] and the Neutral Gas Shielding (NGS) model[6] - see later), which takes into account shielding of the spherical cloud, channel flow and electrostatical double potential[7]. For deposition profiles, a similar comparison were made - using the HPI[8] and PRL[9] simulation codes - at the Mega Amp Spherical Tokamak (MAST) with the main goal of investigating the ∇B-induced pellet cloud drift (which drives the ablated material towards the magnetic Low Field Side - LFS), and its effect on the pellet material deposition. The results were in good agreement with the experiments, except discrepancies between the measurements and one of the applied simulations in some cases[10].

At H-mode operation - which is the planned main operation mode for the International Thermonuclear Experimental Reactor (ITER)[11] - in tokamaks pellets injected in the plasma usually trigger a plasma instability, the so-called Edge Localized Mode (ELM). This is an unfortunate effect in terms of fuelling, since ELM crashes wash out a significant part of the deposited pellet material from the plasma, but this phenomena makes the pellets a good candidate for controlling edge instabilities[12, 13]. However, efficient fuelling is still possible in H-mode using supplementary methods[14, 15, 16, 17].

In order to efficiently design the pellet ELM triggering tool, it's important to understand how a pellet causes a perturbation in the plasma parameters, which then can trigger an ELM. It is experimentally found, that this perturbation is localised radially (appears at the middle of the pedestal)[18] and toroidally[19, 20], which finding was also confirmed by non-linear magnetohydrodynamical simulations[21]. However, investigating this local perturbation, quantitative discrepancies have been found between the experiments and simulations in some cases regarding the minimal number of particles to trigger an ELM[22]. Nevertheless the main source of pellet perturbation causing an ELM seems to be the field line elongated, high pressure pellet cloud (or plasmoid). In this paper, we investigate the properties of this plasmoid.

One of the first direct pellet cloud observations was at the Texas Experimental Toka-

mak (TEXT) and was reported in[23], which made suggestions to refine the theoretical, time independent ablation models (along with the results at the ASDEX tokamak[24]), like the classical NGS model[6]. The reason of this refinement was the experimental observation of pellet cloud striations (periodically changing brighter and darker regions along the pellet path - seen on long exposure images)[25]. At TEXT, pellet clouds were recorded with cameras sensitive in the visible range. The observed main cloud shapes are composed of one or two ellipsoid (parallel with the magnetic field lines) with one brightness peak per ellipsoid. At ASDEX Upgrade, pellet cloud images were used to improve plasma q-profile reconstruction, where similar pellet cloud shapes were reported[26].

On fast video camera recordings, it was observed, that part of the plasmoid surrounding the pellet frequently detaches from the main cloud and drifts towards the magnetic low field side (LFS) with a speed two orders of magnitude higher, than the pellet speed[27, 28]. This drift is likely caused by the ∇B drift and points to the same direction (the outward radial direction) at high field side (HFS) and LFS injections. Moreover, in some cases, high speed drifting cloudlets moving toward the upward vertical direction were also observed[28]. Accordingly, at certain times, two cloudlets can be seen on one snapshot of the recording. One is the cloudlet of the ablating pellet and the other is the cloudlet, which is drifting away, but still radiates in the visible range.

The pellet ELM triggering experiments drew back the attention to the investigation of the distribution of pellet clouds. Our goal is to determine the material- and temperature distribution inside the pellet cloud to make the existing simulations more realistic by providing a more precise distribution of the local perturbation. Furthermore, to apply the results to different machines, it is necessary to make a scaling with the major parameters determining the pellet cloud distribution along the magnetic field lines.

In this paper, individual short exposure time pellet cloud images were analysed based on our recordings with cameras sensitive in the visible range. The main identified cloud shape categories are shown along with a scaling law for the pellet cloud extent on the magnetic field lines as a function of different pellet- and plasma parameters. The simulation of the diagnostic system is introduced (synthetic diagnostic). With the help of this simulation, the material and temperature distribution necessary to produce one of the main observed pellet cloud shapes is described. Moreover, it was analysed, whether the different pellet isotopes (hydrogen, deuterium) and plasma materials (hydrogen, deuterium, helium) introduce any difference in pellet cloud extent in the direction of the magnetic field and perpendicular to it, which is an important question at the start of ITER.

The article is organised as follows. First the experimental setup is described in Sec. 2, then the typical cloud shapes are introduced in Sec. 3. The scheme of the pellet cloud database along with the statistical analysis of the data (containing the scaling for the pellet cloud length) can be found in Sec. 4. Then Sec. 5 contains the description and the results from the synthetic diagnostic. Finally, in Sec. 6 there is a discussion about the presented results.

2 Experimental setup

The ASDEX Upgrade tokamak is a middle-size divertor tokamak with a major radius of 1.65 m, the typical values of configuration are: minor radius of 0.5 m, the plasma volume is 13 m^3, the maximum toroidal magnetic field is 3.1 T. The plasma elongation is typically 1.6-1.8. The plasma facing wall elements were (partly) coated with tungsten until 2007, after that the wall become a full metal (stepwise from 1999 - 2007)[29], tungsten coated wall. The shots analyzed in this article were performed between 2005 and 2012 (the first pulse number in the database 20513, the last is 28503), which means there are shots with the partial carbon and also with the full tungsten coated wall as well. For pellet launch a centrifuge pellet injector[30] was used, the pellets arrived from the magnetic high field side (HFS). The centrifuge is capable to deliver pellets in the velocity range of $240 - 1000$ m/s with a pellet size of $1.7 - 4 \cdot 10^{20}$ D_2 (or H_2) molecules. The schematics of the pellet injection system is seen on Fig. 1. From the centrifuge the pellets fly through a guiding tube to reach the inner side of the tokamak. All the recordings selected for this investigation were made in H-mode plasma with various heating schemes, the most significant part of the heating was provided by the neutral beam injection (NBI) using electron-cyclotron resonance heating (ECRH) and ion-cyclotron resonance heating (ICRH) as coheating.

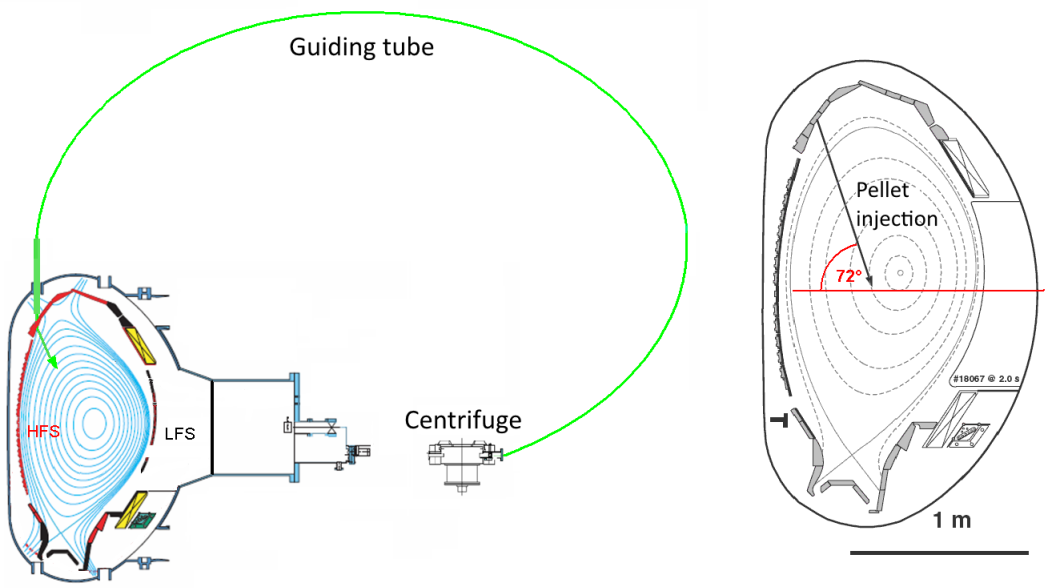

Figure 1: The ASDEX Upgrade centrifuge pellet injection system

The diagnostic system[31] viewing from the 5Co port of the tokamak (the same sector where the pellets are injected), is a radial view facing the inner wall. The light is transported through an image guide (fiber optic matrix) to an optical system (consisting of mirrors and beam splitters) and from there to the CCD chip of a PCO SensiCam. The system has the possibility to use up to three cameras for recording simultaneously at every shot. On every image there are multiple, short exposures, which results in a stroboscope-like recording (multiple pellet clouds on one image, each was taken at different time, and therefore seen at different position; see upper left corner of Fig. 2). The trigger for our cameras were provided by the pellet centrifuge, when it released a pellet. A delay was applied to this trigger to compensate the time, while the pellet flies through the guiding tube. This way, when the (delayed) trigger has arrived, the pellet was near to the vacuum vessel and the camera started to make exposures, typically 10 ms before the pellet arrived. However, the time stamps of the images were synced with the central clock of ASDEX Upgrade, this way the timing of the images is correct. The exposure time was set short - to avoid saturation and blur on the image and to ensure, that we record one snapshot -, it was typically set between 1 - 10 μs. The repetition time between two exposures (on one image) was set so, that the consecutive exposures about the pellet clouds are clearly separated on the images. Depending on the designed pellet velocity, this was typically $60 - 150$ μs.

The whole procedure described above can be seen schematically in Fig. 2. Due to our limited view to the pellet path, the dataset contains clouds, which were photographed

at poloidal flux surfaces between 1 and 0.76 (which is equivalent with the 18.5 - 52.4 cm distance range measured from the pellet injection point).

All the images were spatially calibrated - with the precision of a few millimeters - using the camera obscura model, and the individual pellet clouds were separated. At the spatial calibration it is assumed, that the whole ablation process takes place on a plane, which is spanned by the line of the designated pellet path and the magnetic field lines in the vicinity of this line. This seems to be a reasonable assumption according to the camera measurements from the 4Co (tangential view)[32], at least from the injection point to the 0.76 poloidal flux surface, where our datapoints are located.

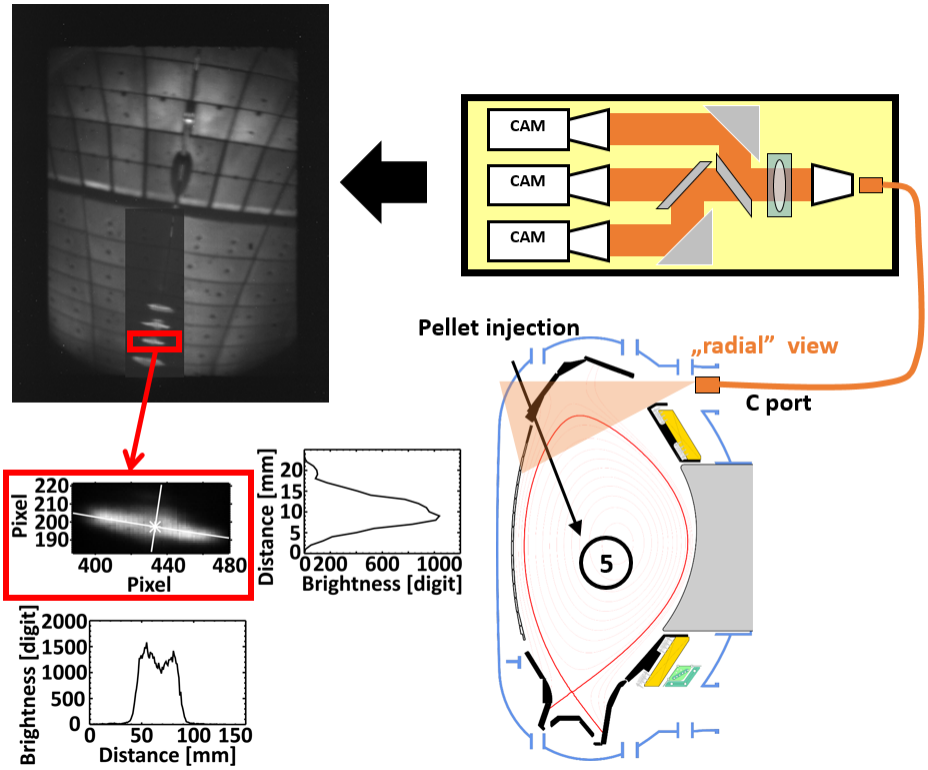

Figure 2: The diagnostic system and data flow to the database. Lower right: toroidal cross-section with the pellet path and the diagnostic system. Upper right: schematics of the observation system. Upper left: an example of the stroboscope-like recordings with the individual pellet clouds taken at different time during the pellet flight (in order to visualize both, the pellet cloud snapshots are overplotted to the bright image of the inner wall of the vessel). Lower left: the extracted individual pellet cloud with the pellet path and the magnetic field line crossing the geometrical centre of the cloud, brightness distributions along the pellet path and along the field line.

3 Typical cloud shapes

In this section the typical observed cloud shapes are introduced. 96% of all observed clouds can be aligned into four, empirically assigned main shapes (classes). For all the latter displayed images, the almost vertical line represents the designated pellet path, and the almost horizontal line is the magnetic field line crossing the middle of the cloud. The centre of the cloud is the geometrical centre (or centre of gravity), not always the highest radiation region. The typical cloud extent (full width of the brightness distribution at half of the maximum - FWHM) is 1 - 9 cm along the magnetic field line crossing the centre of the cloud(let) and 0.5 - 2 cm perpendicular to the field line. After investigating the camera images, the following, empirical classification of the pellet clouds was found.

Shape I: "classic“, cigar-shape cloud with one radiation maximum along the magnetic field line (see Fig. 3; the coordinates of the magnetic field line is marked with z). This cloud shape was also observed by Durst et al.[23] and also Müller et al.f[26].

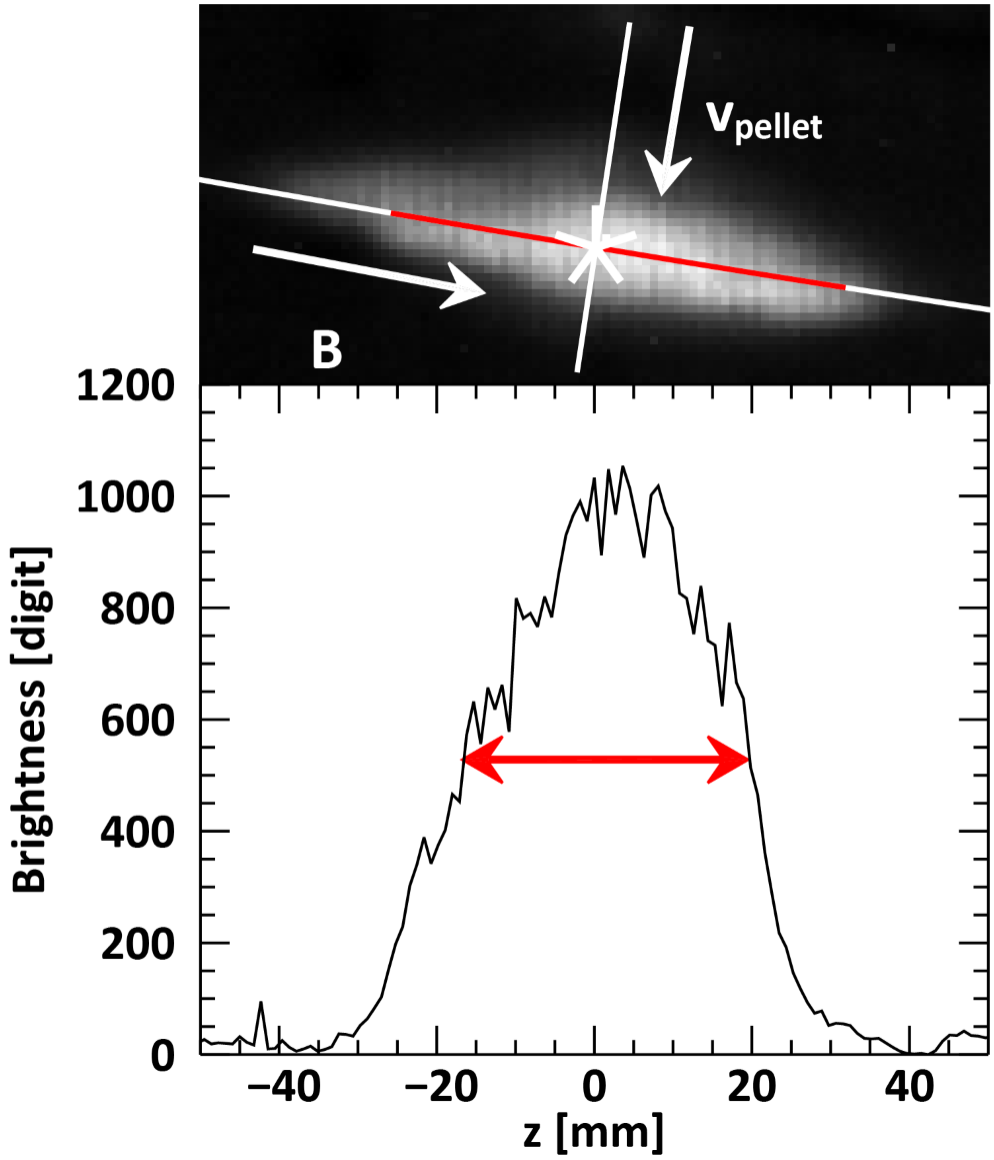

Figure 3: Top: Image of the shape I cloud; bottom: brightness distribution along the magnetic field line marked on the cloud.

Shape II: Cigar-shape with two radiation maxima (see Fig. 4). This was also observed in [26] in some cases (though it hasn't been introduced as a separate category), but hasn't been reported in [23]. The distributions producing this shape will be further discussed in Sec. 5.

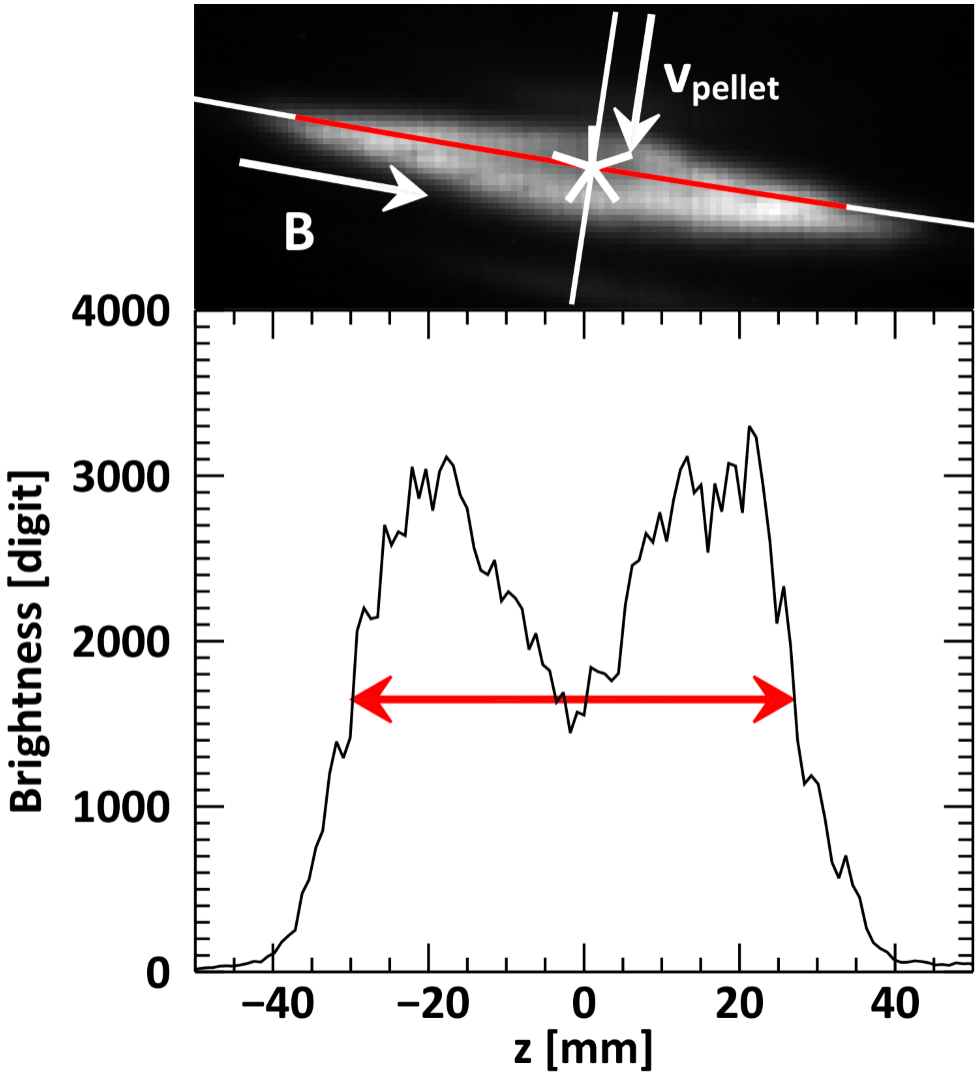

Figure 4: Top: Image of the shape II cloud; bottom: same as in Fig. 3.

Shape III: Two cigar shapes, each with one radiation maximum (see Fig. 5). This shape was also reported in both [23, 26]. The cause of this shape is (according to [28]) the drift caused by the gradient of the magnetic field, which pushes the cloudlet towards the LFS with a much higher speed, than the pellet velocity. However, [26] reported, that at AUG, an upward component of this drift was also observed. A recent investigation confirms this observation[28].

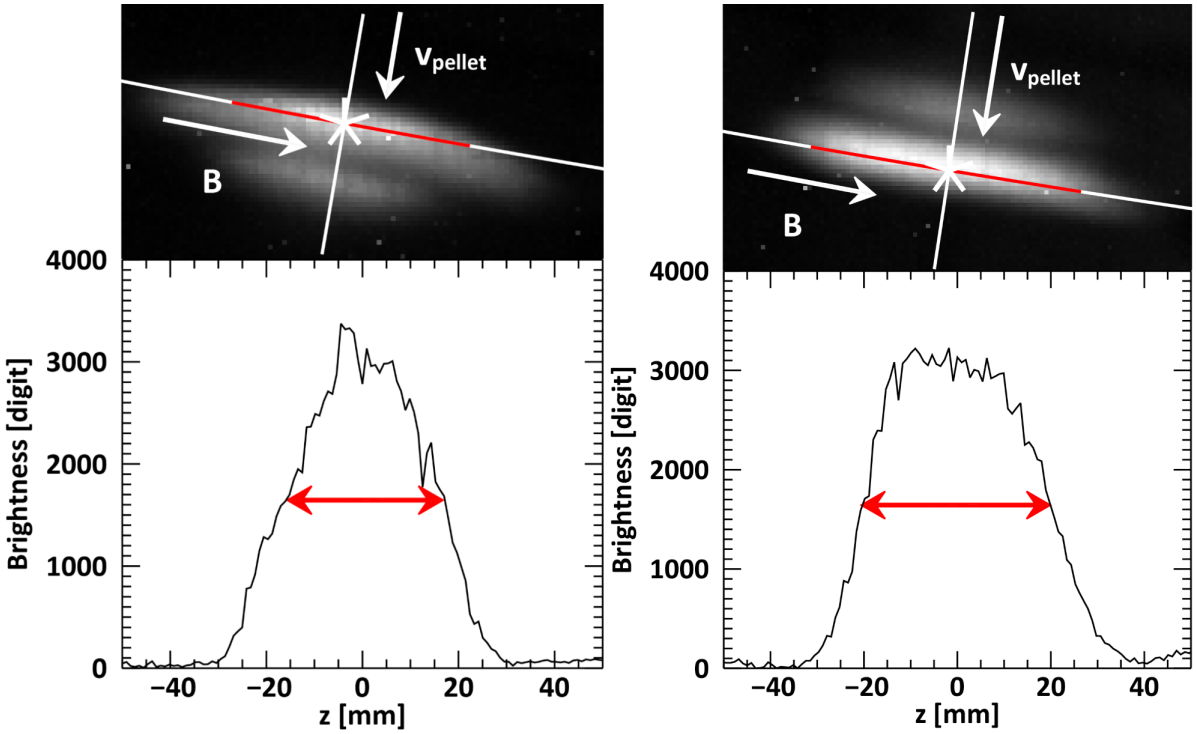

Figure 5: Image of the shape III cloud. Left: the upper cigar is brighter and wider. Right: the lower cigar is brighter and wider.

Shape IV: Two cigar shapes with several radiation maxima (see Fig. 6). This shape hasn't been reported yet. There are two subtypes of this cloud shape; the first is with two radiation maxima on the upper cloud and one on the lower one; the other is the opposite.

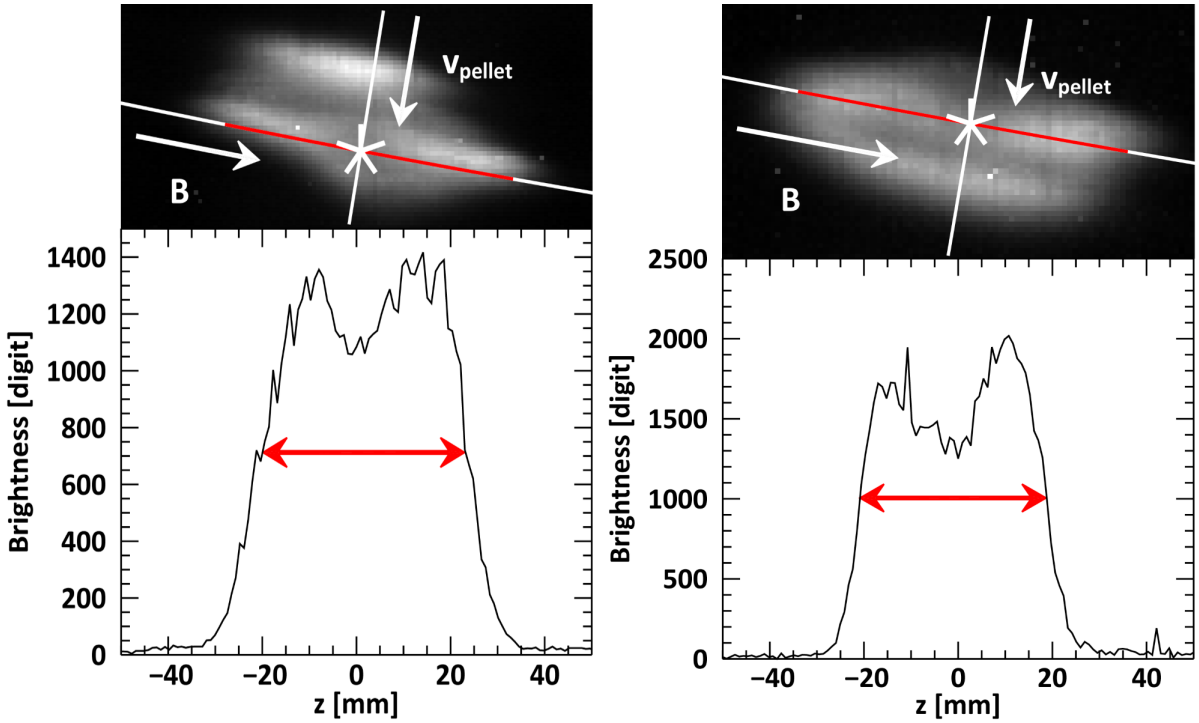

Figure 6: Image of the shape IV cloud. Left: two maximum at the lower, and one maximum at the upper cigar. Right: one maximum at the lower, and two at the upper cigar.

4 The pellet cloud database

With the observation system described in Sec. 2, images were collected from several experiments. These experiments were typically pellet fuelling and pellet ELM control in standard or nitrogen seeded H-mode in deuterium, helium and hydrogen plasmas. The collection method of the images are also described in Sec. 2. After the collection, separation of the pellet clouds and the spatial calibration, the coordinates of the centre of each cloud were determined, that can be represented in flux surface labels, cylindrical coordinates etc. The initial local values of the corresponding quantities (magnetic field strength, plasma temperature and density etc.) were also collected. The local values of the temperature and density are based on reconstructed profiles before the pellet arrival into the plasma. Using the collected data, the extent, and brightness distribution of the clouds were determined along the direction of the magnetic field lines and perpendicular to it through the geometrical centre of the cloud - as can be seen in Fig. 2 (around the red box). At clouds with two cloudlets (called shape III and IV in Sec. 3), the brighter stripe (along the magnetic field lines) was investigated based on the assumption, that the pellet is the primary particle source of the cloud, so the

brighter cloud encompasses the pellet (since it is colder, thus emits more visible light). From all of this collected data, a database was built, which contains pellet-, cloud- and plasma specific information for all of the 254 observed pellet cloud. The fields in the database can be categorized based on type (plasma, pellet or pellet cloud parameters) and dimension (a value, a vector or an array), see Tab. 1.

The only two-dimensional data field in the database is the image of the pellet cloud itself. The one-dimensional fields in the database are the following. Concerning the plasma parameters, these are the flux coordinates $(\rho_{pol.}(l))$ along the pellet path (l), the electron density $(n_e(l))$ and temperature $(T_e(l))$ profiles calculated a few ms before the pellet arrival to the plasma. For the pellet parameters, these are the pellet path in physical coordinates (l), the pellet size $(r_p(l))$ and the ablation rate $\left(\dot{N}(l)\right)$ along the pellet path.

The pellet size at the location of the cloud $(r_p(l_c))$ and along the whole pellet path $(r_p(l))$ was calculated from the reduced size, which is empirically estimated for different pellet speeds and nominal sizes and describes the pellet deterioration in the flight tube, and therefore gives the pellet size at the torus entrance[30]. The calculation for the reduced pellet size takes into account, that at higher speed, the pellet mass deterioration is also higher in the flight tube, even at the same initial mass. The ablation rate $\left(\dot{N}\right)$ inside the torus based on the NGS model[6] is

$$\dot{N} = 1.12 \cdot 10^{16} \cdot r_p^{\frac{4}{3}} \cdot n_e^{\frac{1}{3}} \cdot T_e^{1.64} \cdot M_i^{-\frac{1}{3}} \tag{1}$$

where the ablation rate is measured in $\left[\frac{atoms}{s}\right]$, r_p is in $[cm]$, the unit of n_e is $[cm^{-3}]$, the plasma electron temperature is in $[eV]$, and M_i - the atomic mass is in $[atomic\,units]$. The ablation rate in this whole paper is calculated from Eq. 1. This means, that the calculated ablation rate will inherit the uncertainty of the plasma temperature and density, however, for the investigated shots this is the most reliable method to evaluate the material decrease of the pellet.

For the pellet cloud the one-dimensional parameters are the coordinates of the magnetic field line (z) crossing the geometrical centre of the cloud and also a vector holds the horizontal and vertical cloud brightness distributions (digit level vs. distance along the magnetic field line and in the perpendicular direction, respectively).

The single fields corresponding to the plasma parameters are the shot number, the plasma material (deuterium, hydrogen or helium), the power of the various applied heating powers (NBI, ICRH, ECRH, Ohmic) at the recording time of every image. By using the applied heating power instead of the absorbed heating power can introduce uncertainties, however, the heating powers will not be used in this paper for analysis.

The time windows, in which the temperature and density profiles are determined (these can differ for density and temperature profiles) are also stored. As of pellet parameters, the nominal size - which is the designated size of the pellet, when it leaves the centrifuge - and the reduced size are stored along with the pellet material (deuterium or hydrogen). The pellet speed, which is taken as constant during the whole ablation process and equal to the designated speed is also stored. Using the designated pellet speed means, that the radial pellet acceleration in the plasma - described by the rocket model -, and the acceleration caused curvature of the pellet path is neglected. This is a reasonable assumption here (see [32]), because at the separatrix - where the profiles are steep - the effect of the acceleration is small, so it can be neglected. Deeper in the plasma the curvature is larger, but the profiles are shallower, therefore the temperature and density values does not change as much. The ablation rate at the position of the pellet cloud (l_c) is also stored, which was calculated from the NGS model (see Eq. 1). The local, unperturbed plasma electron density and temperature at the position of the pellet is also part of the database and calculated from the reconstructed profiles. Concerning the pellet cloud parameters, the single data fields contain the name of the recording camera, the exposure time, the repetition time between two exposure cycle, the trigger time of the camera image corresponding to the actual cloud, the image number in the recording loop, the cloud position in physical coordinates (l_c). The first four moments of the horizontal- and vertical cloud brightness distributions are also calculated and stored. The horizontal- and vertical cloud size (full width of the brightness distributions at half maximum) and the cloud shape - which was discussed in more details in Sec. 3 - are also in the database.

Dim.	Plasma params.	Pellet params.	Pellet cloud params.
0	shot number	nominal size	camera name
	plasma material (D, H, He)	reduced size	exposure time
	NBI heating power	material (D, H)	repetition time
	ICRH heating power	speed (v_p)	trigger time
	ECRH heating power	ablation rate $\left(\dot{N}\left(l_c\right)\right)$	image number
	Ohmic heating power	electron density ($n_e\left(l_c\right)$)	cloud number
	temperature profile time	electron temperature ($T_e\left(l_c\right)$)	cloud position (l_c)
	density profile time	size ($r_p\left(l_c\right)$)	cloud brightness distribution moments (along z)
			cloud brightness distribution moments (along l)
			cloud size along z (FWHM)
			cloud size along l (FWHM)
			cloud shape
1	flux coord. ($\rho_{pol.}(l)$)	pellet path (l)	magn. field line coords (z)
	electron density profile ($n_e(l)$)	pellet size ($r_p(l)$)	cloud brightness distribution along z
	electron temperature profile ($T_e(l)$)	ablation rate $\left(\dot{N}(l)\right)$	cloud brightness distribution along l
2			cloud image

Table 1: Summary of the parameters stored in the pellet cloud database

From the collected information a scaling - which is aimed to reveal the connection between the different pellet- and plasma parameters and the pellet cloud width - will be derived. The available ranges in the database of these parameters can be seen in Tab. 2. Since the source of the material forming the cloud is the pellet itself, and the amount of this material is determined by the pellet ablation, it is important to know, how the extension of the pellet cloud is connected to the ablation rate. However, there might be other important parameters describing the pellet cloud length, such as the pellet speed, which is one of the main pellet parameters. It is also worth to investigate the parameters from Eq. 1 separately, since the weight they contribute to the cloud length can be different from their contribution to the ablation rate. But first, we make

$v_p\ \left[\frac{m}{s}\right]$	$V_p\ [mm^3]$	$T_e\ [eV]$	$n_e\ [10^{19}\ m^{-3}]$	$\dot{N}\ [10^{23}\ s^{-1}]$
240, 255, 560, 600	0.4 - 3.68	37 - 787	1.3 - 8.1	0.03 - 4.10

Table 2: Ranges of the most important parameters in the database. The pellet speed (v_p) is the designed value, all the other parameters are measured $(T_e,\ n_e)$ or calculated $\left(V_p,\ \dot{N}\right)$ locally, a few milliseconds before the pellet arrives to the plasma.

an attempt to find the most important parameter in view of the pellet cloud size.

In the database, most of the data is originated from deuterium plasma with deuterium pellets. In the next few paragraphs, only this part of the database will be discussed. First, it is investigated, how the cloud length is connected to the ablation rate. The data plot about this can be seen on Fig. 7.

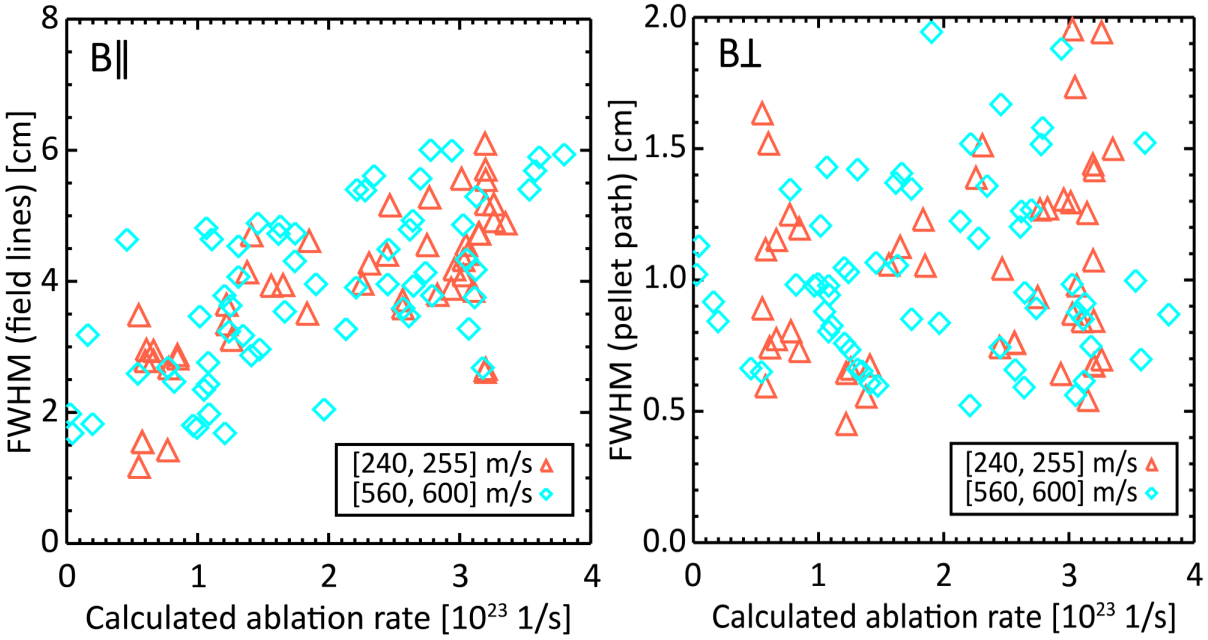

Figure 7: Pellet cloud width - ablation rate. Red triangles mark the [240, 255] m/s, cyan diamonds mark the [560, 600] m/s pellet speed. Left: cloud size along the magnetic field line vs. ablation rate. Right: cloud size perpendicular to the magnetic field line vs. ablation rate.

On the left-hand side of Fig. 7 a trend is visible: with higher ablation rate, the pellet cloud is wider along the magnetic field lines. This trend cannot be seen perpendicular to the field line (right side of Fig. 7). Based on this observation, the rest of the figures will deal only with the cloud size along the magnetic field line (except at the investigation of the isotope effect). It is worth to mention, that while the cloud length along the magnetic field line is definite at shapes I and II (see Sec. 3), there are multiple possibilities at the other cloud shapes. At these cases it is assumed, that one of the

stripes comes from the drifting cloudlet, and the other one contains the pellet itself. This latter stripe is considered to be the brighter one and this is chosen to represent the cloud width.

Investigating the FWHM - remaining pellet volume plot (which is equivalent of the pellet mass knowing the density of the solid deuterium and assuming spherical shape for the pellet) one can observe, that with higher pellet volume the cloud width decreases according to a complicated function with possible hidden parameters (see Fig. 8), which tends to depend on the pellet velocity too. There are three distinct regions (at 2, 3 and 3.7 mm^3), where it seems, that the cloud width varies much without a large change in the pellet volume at a given velocity region.

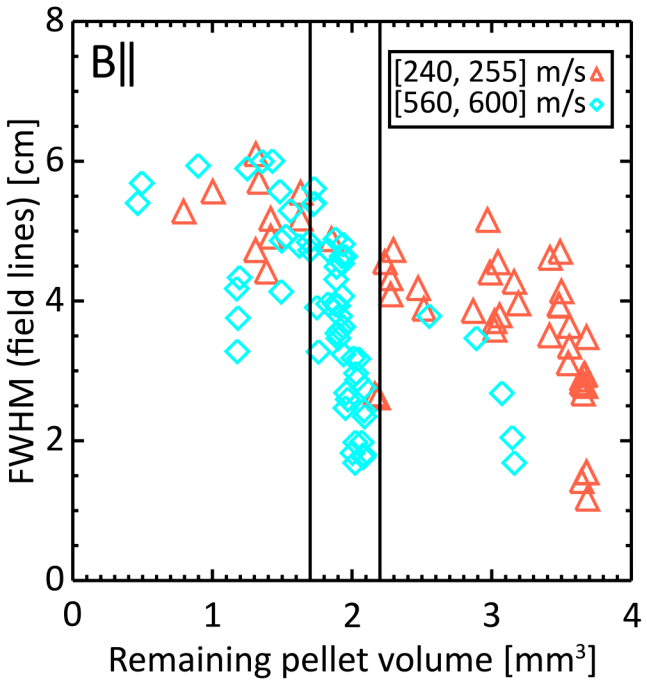

Figure 8: Pellet cloud width as a function of the remaining pellet volume (approximated with a sphere). Red triangles: [560, 600] m/s pellets, cyan diamonds: [240, 255] m/s pellets. The region defined by the two vertical lines contains the points, which are used in Fig. 9.

Since the FWHM inherently contains the effect of the temperature and density e.g. through the NGS ablation rate formula (as mentioned above), points from the 2 mm^3, $[560,\ 600]\ \frac{m}{s}$ region were chosen to investigate the FWHM - temperature connection at a (fairly) constant pellet volume. This region contains the most points, so it is a good candidate to look for the connection with the temperature and density.

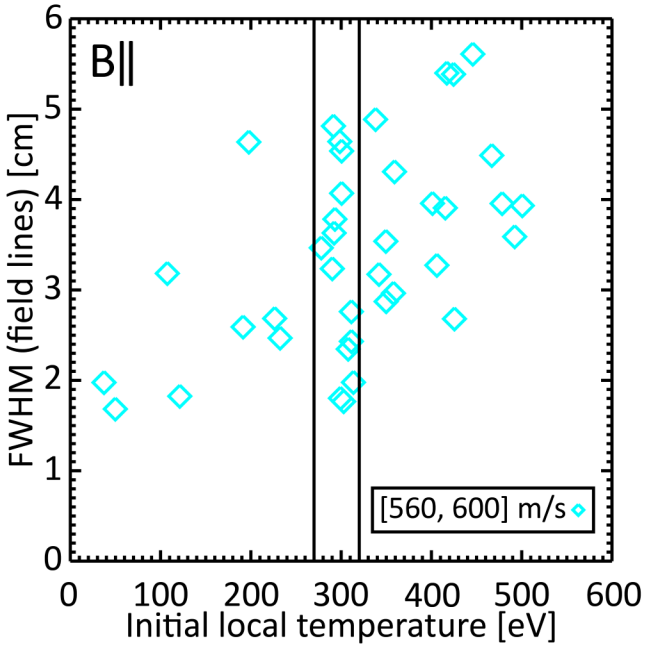

Figure 9: Cloud width as a function of initial (unperturbed background plasma) local temperature for the selected points in Fig. 8. Only the clouds originated from [560, 600] m/s pellets are shown.

We investigated the cloud lengths originated from $[560,\ 600]\ \frac{m}{s}$ pellets (where we have enough data points) and they clearly show an increasing trend with increasing temperature (this can be seen in Fig. 9). This trend can be a combined effect of the density and temperature, since the effect of the density is still not filtered from the plotted data points. By filtering the data further for a (fairly) constant temperature range, the contribution of plasma electron density can be plotted (see Fig. 10). It can be seen, that the FWHM depends on the density in a nonlinear way. Summarily, it seems, that the pellet cloud width seems to increase with decreasing pellet volume, and increasing plasma electron density and temperature, however, the connection is rather nonlinear, which needs to be further investigated.

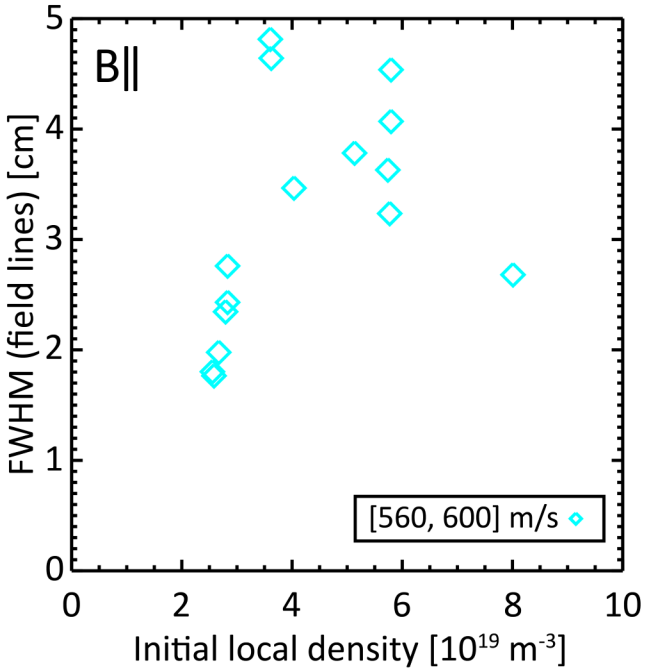

Figure 10: Cloud width as a function of initial local (unperturbed background plasma) density for the selected points in Fig. 9. Only the clouds originated from [560, 600] m/s pellets are shown.

To summerize and clarify the observations based on the plots shown above (Figs. 7, 8, 9 and 10) a scaling for the cloud length (FWHM) along the magnetic field lines was derived based on the data shown. This scaling - based on the NGS model - was derived in two forms. The first form contains the pellet speed and volume, the plasma electron density and temperature separately in the form of power functions using the following equation Eq. 2.

$$l_{FWHM} = C \cdot v_p^{\alpha_1} \cdot V_p^{\alpha_2} \cdot Te^{\alpha_3} \cdot ne^{\alpha_4} \tag{2}$$

The decision of using power functions is based on the NGS model, which is very successful in describing the ablation rate, despite its simplicity. Since we assume, that the ablation rate is important in determining the cloud length, we also look for the scaling in this form.

The other equation contains only the pellet speed (the only quantity from right-hand side of Eq. 2, which is not present in the NGS-model) and the ablation rate ($\dot{N}$), also in a power function form (see Eq. 3).

$$l_{FWHM} = C \cdot v_p^{\alpha_1} \cdot \dot{N}^{\alpha_2} \tag{3}$$

A nonlinear fitting was used for both equations 2 and 3. The results can be seen in Table 3. It was crosschecked with a linearized polinomial fitting and the resulting coefficients were matching within error. The values in parentheses are calculated from the NGS model (Eq. 1).

	v_p	$\dot{N}$	V_p	Te	n_e	const.	χ^2
Eq. 3	0.05 ± 0.05	0.34 ± 0.05	(0.15 ± 0.02)	(0.55 ± 0.08)	(0.11 ± 0.02)	3.0 ± 0.3	0.772
Eq. 2	-0.03 ± 0.05	—	-0.09 ± 0.04	0.40 ± 0.05	0.13 ± 0.08	1.0 ± 0.2	0.691

Table 3: Parameters of the different fitting methods. The fit based on Eq. 3 is written as abl. rat. and the fit based on Eq. 2 is marked as all params. The coefficients in parentheses are calculated based on the ablation rate formula of the NGS model (see Eq. 1).

It can be seen from both fits, that the temperature has the most significant impact on the cloud width, with coefficients 0.55 and 0.4 (based on Eq. 3, Eq. 2, respectively). The possible cause of the temperature dependence is that the material source of the cloud is the pellet itself. The rate of the material flowing to the cloud is given by the ablation rate. According to the NGS model, the ablation rate has a power dependence from the background plasma temperature with the exponent of 1.64. Since this is the highest exponent, it is expected, that the temperatures has the highest influence on the cloud length.

The effect of the pellet velocity seems to be negligible, since it is 0.05 with the ablation rate fit and -0.03 with the all parameters fit and within error, both fit allows it to be zero. This is consistent with the idea, that the pellet provides the material for the cloud according to the NGS model and the model does not depend on the pellet speed.

It seems, that the density has only a slight contribution – which can also be derived similarly to the temperature dependence –, which agrees (within error) for both fits and is around 0.1, however, the Eq. 2 fit gives a quite large error. The most ambiguous parameter is the pellet volume. For this, the two methods give the coefficients 0.15 and -0.09, respectively. The reason for the different sign is a subject for further investigation, but it can be stated, that the ablation rate fit does not allow the pellet volume to be negative alone, since it has a positive sign for all the coefficients. It means, that either all of the parameters (the whole ablation rate coefficient) or none of the calculated parameters can be negative. Comparing this with the all parameters fit shows, that the large positive power of the density and temperature in the all parameters fit does not let the ablation rate to have a negative coefficient in the power function, but since the value of χ^2 is slightly closer to 1 for the ablation rate fit case, it indicates, that the pellet volume might have a small positive influence on the cloud width rather

than negative. However, based on the small difference of χ^2 between the two fits, it cannot be easily decided, which one fits the dataset better. Although the ablation rate provides the source of the pellet cloud and since there is no big difference between the two methods, the use of the ablation rate seems more practical.

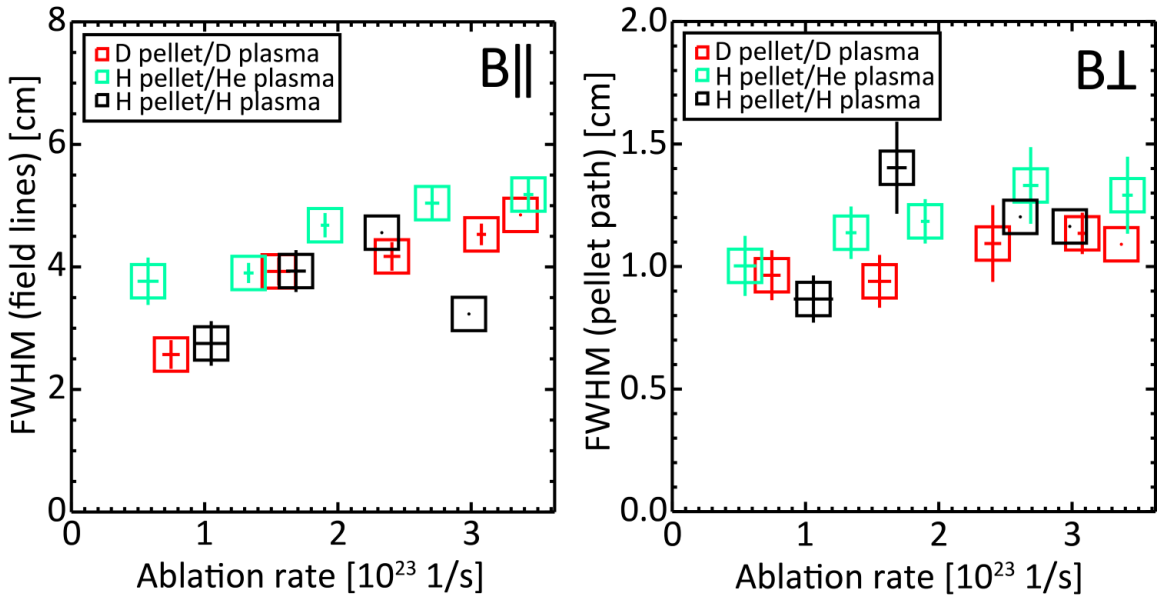

Figure 11: Investigation of the isotope effect with different pellet- and plasma combinations. The pellet velocity shown here is 240 m/s, since for the H/H and H/He data only contains this speed value.

It is also important to know, whether the above reviewed characteristics differ for different isotopes and background plasma. For example, ITER will start its operation with helium plasma and hydrogen pellets. Thus, it was investigated, whether the hydrogen pellet clouds in helium or hydrogen plasma show the same behaviour with the cloud FWHM or there is a difference compared to the „standard“ deuterium pellet in deuterium plasma case. The statistical analysis shows, that the trend is the same as the usual deuterium plasma and deuterium pellets case. The averaged values are shown on Fig. 11. Along the x axis even spacing was used and the values in a box were averaged along the y direction. The errors both in x and y direction were the standard deviation. Unfortunately, for the hydrogen pellet - hydrogen plasma case, the database contains only one shot (#28503) with 21 pellet clouds. In the other cases, there are considerably more events collected (113 for the hydrogen pellet - helium plasma case, and 60 events for the deuterium pellet - deuterium plasma case). This is a subset of the whole database, since only the clouds of pellets with the velocity 240 m/s were used, since the H/H and H/He configuration only contained 240 m/s pellets. However, it can

be stated, that (within the uncertainty of the measurements) there is no difference in terms of pellet clouds by using D/D, H/H and H/He pellet/plasma configuration. The main cloud shapes (described in Section 3) are also observable in all cases.

5 The synthetic diagnostic

In the previous section the distribution of the pellet cloud visible light emission was investigated experimentally. However, first principle models usually simulate the pellet cloud properties, e.g. the distribution of the electron density, temperature and ionisation degree. To link the results of these model calculations to the measurement, a synthetic diagnostic has been developed, which calculates the light emitted by the simulated pellet cloud, based on pellet- and plasma parameters. On the other hand, the synthetic diagnostic helps us to estimate the physical parameters of the cloud from the acquired camera images.

When developing the synthetic diagnostic, our approach was the following. We assumed, that the electron density, temperature and ionization degree of the pellet cloud particles are prescribed (inputs from a model) along the magnetic field line. It was also assumed, that the pellet cloud is cylindrically symmetric around the magnetic field line crossing the middle of the pellet cloud. The distribution of the cloud parameters perpendicular to the magnetic field line is not really given by the models, therefore several approaches were tested, and the one which gives simulated radiation distribution similar to the measured ones was finally selected. The simplest approach tested was, when no gradient in the distribution perpendicular to the magnetic field was assumed. Another approach assumed that the parameters have an exponential decay in the perpendicular direction. These distributions gave qualitatively different pellet cloud images as the observed ones. The most successful approach was the so-called quasi two-dimensional (Q2D) one[33], which mimics the transformation of the spherical expansion of the neutral pellet cloud into the channel flow along the magnetic field lines. The applied flow pattern is seen on Fig. 12.

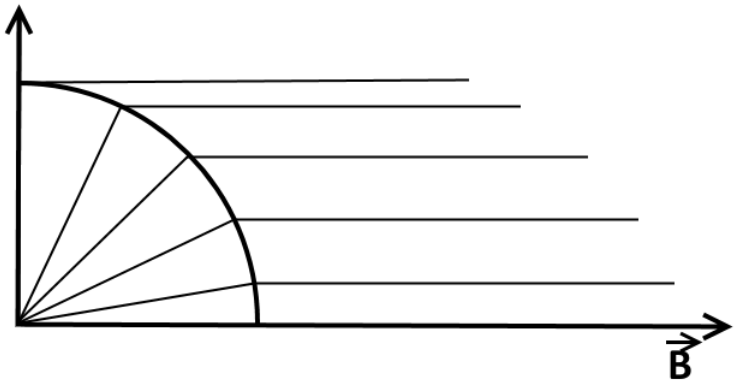

Figure 12: The scheme of the most successful Q2D approach (the figure shows one fourth of the full 2D distribution, however, the distribution is symmetric for both axes shown here).

The inevitable parameter, the typical radius of the spherical cloud was taken from the experiments as 1 cm. The two dimensional distribution of the pellet cloud parameters were determined taking the distance from the pellet according to this flow pattern. These two dimensional distributions were used to compute the three dimensional parameter distributions in the pellet clouds by assuming cylindrical symmetry. The three dimensional distribution of the light emission of the pellet cloud was calculated by a collisional-radiative model[34]. Since the measurement did not use wavelength selection, the total radiation in the visible range was calculated. The last element of the synthetic diagnostic code then mimics the measurement itself by projecting the calculated radiation to a two dimensional plane using the camera obscura model.

The goal of the synthetic diagnostic was to restore at least one of the observed cloud shapes from the output of pellet cloud simulations. The only simulation, whose results resemble the observed small pellet cloud size along the field line (5-10 cm) and whose parameter distributions are available was the hybrid code. That code takes into account both the spherical pellet cloud expansion and the field aligned channel flow. For the present analysis, the results from [35] (one dimensional distribution of the cloud atom- and electron density and electron temperature) were used (see Fig. 13).

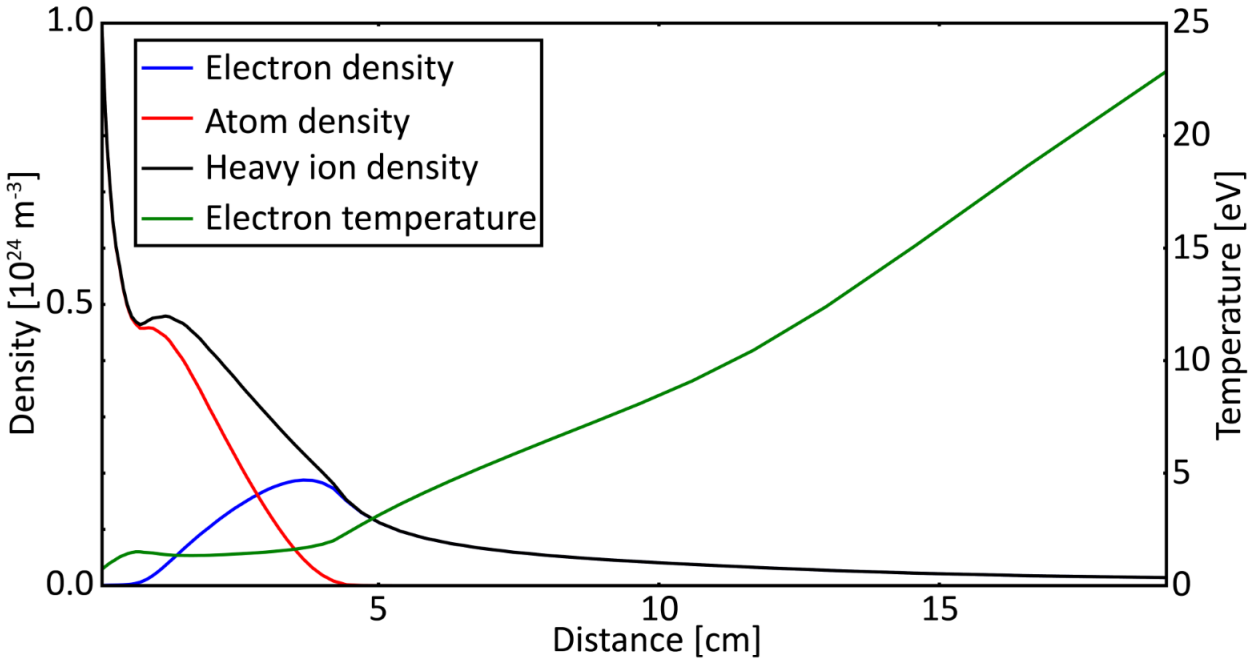

Figure 13: One dimensional distributions for the synthetic diagnostic.

This model calculation was performed for ASDEX Upgrade geometry. The unperturbed plasma density and temperature was $10^{19} m^{-3}$ and $800 eV$, respectively, while the pellet size and speed was $2.14\ mm^3$ and $500\ \frac{m}{s}$, respectively. These results were taken at a time instant when the pellet cloud is already well developed, in other words, both the spherical neutral, and the field aligned ionised pellet clouds were well developed, reaching a stationary state. At this phase - as it can be seen on Fig. 13 - the atomic density drops rapidly when moving away from the pellet surface along the magnetic field line.

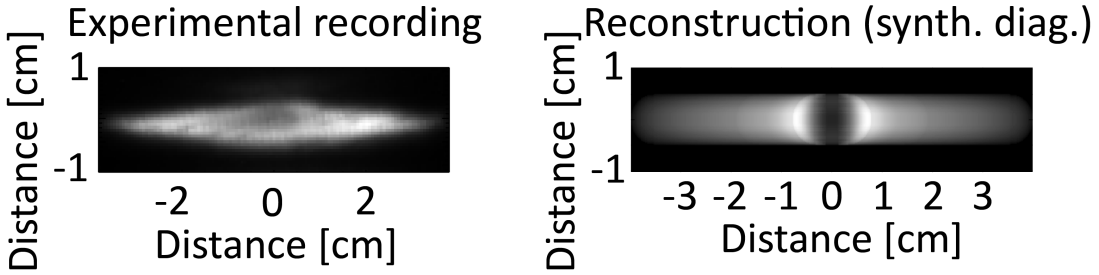

Figure 14: Left: an original recording of the „cigar“ cloud shape with two radiation maxima. Right: the reconstructed cloud shape with two radiation maxima.

On the other hand, according to the ongoing electron impact ionisation, the electron density increases, reaches its maximum around 4 cm, then slowly decreases. The line radiation - which is one of the determining light emission method - is proportional both

to the electron and the atomic density, therefore it is not surprising, that the radiation pattern obtained has two maxima along the field lines as plotted on Fig. 14 (the results of the synthetic diagnostic is shown on the right).

It can also be seen, that thought the two images does not agree perfectly, the main characteristics are the same. These characteristics are the dark centre and the two radiation maxima along the magnetic field line (which is shown on the original image and is parallel to the x axis on the synthetic image, and goes through the centre of the cloud).

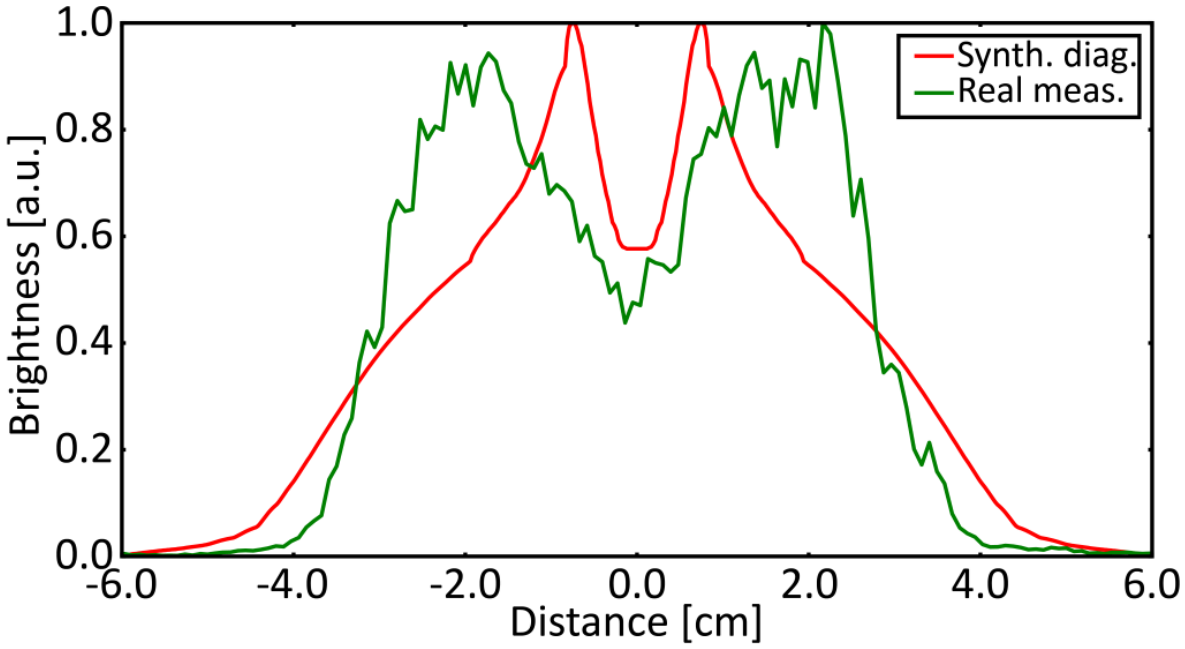

Figure 15: Comparison plot of the simulated (red) and the measured (green) cloud brightness distribution along the magnetic field line.

Looking at Fig. 15 one can see the comparison plot of the brigthness distribution along the magnetic field line for the simulated cloud (red) and the real measurement (green). It can be seen, that - on this normalized plot - the darkness of the middle is almost at the same level. However, the location of the two brightness peaks differ a bit - on the simulated image they are closer to each other. The width of the distribution is essentially the same, but the measured distribution has a steeper decrease on the edge. This means, that the applied simulation or the two- and three-dimensional generation methods can also be improved, but it also gives a fair agreement with the measured distribution.

6 Discussion

From fast visible camera images, a pellet cloud database has been established, which contains the cloud and the related global and local pellet- and plasma information (plasma temperature, density, pellet velocity, pellet volume, ablation rate etc.). From the images the main cloud shapes were derived as an empirical approach. The effect of different isotopes were investigated to the ablation process and the results show, that there is no significant difference between the different isotopes in terms of pellet cloud properties. This means that no effects are expected in the pellet ablation using different hydrogen isotopes as pellet- or plasma material (the investigation also includes the effect of helium plasma).

Using the collected dataset and different fitting methods, a scaling was derived for the length of the pellet cloud as a function of pellet- and plasma related parameters. The results show, that the electron temperature has the highest influence on the length of the pellet cloud, and the coefficient is between 0.4-0.6. This means that ten times higher temperature only causes a three times increase in the cloud length.

To reveal the underlying pellet cloud density and temperature distributions of the observed visible light radiation distribution, a synthetic diagnostic has been developed, which simulates the measurement process, takes its input from pellet cloud simulations and generates similar outputs to the observed camera images. This way it makes possible to compare the outputs of pellet cloud simulations with the experimental observations. As input data for the synthetic diagnostic, the pellet cloud parameters were taken from the hybrid code. The hybrid code simulates the pellet cloud for the case, when the radiation is governed by the cloud electrons, which have much higher density, than that of the target plasma. In this case, a cigar shaped cloud with two radiation maxima along the field line was reconstructed, which reveals that the ionised, field-aligned pellet cloud part is inevitable to be able to observe such a cloud pattern. We believe, that to obtain a pellet cloud pattern with one radiation maximum is only possible, if this ionised pellet cloud part - that is the cloud electrons - is not dominant. Probably, this happens, if the ionised cloud part is detached, and drifting away - caused by the magnetic field gradient -, and leaving mostly the neutral part of the cloud around the pellet. In this case, probably the target discharge electrons dominate the radiation processes, which results in a single-maximum light distribution.

Running the synthetic diagnostic with density- and temperature distributions coming from a simulation we experienced fair agreement between the calculated and the experimental two-dimensional brightness distribution (see Fig. 14). Then, using the simulation data, the electron pressure of the cloud was calculated and normalized

with the background plasma electron pressure used in the simulation. The calculation shows, that there are two maxima of the pressure in the cloud, which are located at 5 cm (measured from the middle of the cloud), where it is 45 times the pressure of the background plasma and it stays above 10 times the background plasma until 6 m along the magnetic field line. This means, that the two maxima of the pressure perturbation are at around the edge of the visible cloud - the location of these maxima can be estimated using the above mentioned scaling of the pellet cloud length - and the whole (including the fully ionized part of the) pellet cloud length can be more than 10 m at a machine similar to ASDEX Upgrade in size.

7 Acknowledgement

This work has been carried out within the framework of the EUROfusion Consortium and has received funding from the Euratom research and training programme 2014-2018 under grant agreement No 633053. The views and opinions expressed herein do not necessarily reflect those of the European Commission.

References

[1] P. T. Lang, K. Büchl, M. Kaufmann, R. S. Lang, V. Mertens, H. W. Müller, and J. Neuhauser. High-efficiency plasma refuelling by pellet injection from the magnetic high-field side into asdex upgrade. *Phys. Rev. Lett.*, 79:1487–1490, Aug 1997.

[2] R Sakamoto, J Miyazawa, H Yamada, S Masuzaki, A Sagara, et al. Pellet fuelling requirements to allow self-burning on a helical-type fusion reactor. *Nuclear Fusion*, 52(8):083006, 2012.

[3] PT Lang, A Lorenz, V Mertens, JC Fuchs, J Gafert, O Gehre, O Gruber, G Haas, M Kaufmann, B Kurzan, et al. Refuelling performance improvement by high speed pellet launch from the magnetic high field side. *Nuclear fusion*, 41(8):1107, 2001.

[4] E Belonohy, OJWF Kardaun, T Feher, K Gal, S Kalvin, G Kocsis, K Lackner, PT Lang, J Neuhauser, et al. A high field side pellet penetration depth scaling derived for asdex upgrade. *Nuclear Fusion*, 48(6):065009, 2008.

[5] LL Lengyel, K Büchl, G Pautasso, L Ledl, AA Ushakov, S Kalvin, and G Veres. Modelling of impurity pellet ablation in asdex upgrade (neon) and wendelstein w7-

as (carbon) by means of a radiative (killer') pellet code. *Nuclear Fusion*, 39(6):791, 1999.

[6] PB Parks and Re J Turnbull. Effect of transonic flow in the ablation cloud on the lifetime of a solid hydrogen pellet in a plasma. *Physics of Fluids (1958-1988)*, 21(10):1735–1741, 1978.

[7] K Gál, É Belonohy, G Kocsis, PT Lang, G Veres, et al. Role of shielding in modelling cryogenic deuterium pellet ablation. *Nuclear Fusion*, 48(8):085005, 2008.

[8] B Pégourié, V Waller, H Nehme, L Garzotti, and A Géraud. Homogenization of the pellet ablated material in tokamaks taking into account the gradb-induced drift. *Nuclear fusion*, 47(1):44, 2007.

[9] PB Parks, WD Sessions, and LR Baylor. Radial displacement of pellet ablation material in tokamaks due to the grad-b effect. *Physics of Plasmas (1994-present)*, 7(5):1968–1975, 2000.

[10] L Garzotti, L Baylor, F Köchl, B Pégourié, M Valovič, KB Axon, J Dowling, C Gurl, GP Maddison, H Nehme, et al. Observation and analysis of pellet material gradb drift on mast. *Nuclear Fusion*, 50(10):105002, 2010.

[11] K Ikeda. Progress in the iter physics basis. *Nuclear Fusion*, 47(6), 2007.

[12] PT Lang, GD Conway, Th Eich, L Fattorini, O Gruber, LD Horton, S Kalvin, A Kallenbach, M Kaufmann, G Kocsis, et al. Elm pace making and mitigation by pellet injection in asdex upgrade. *Nuclear Fusion*, 44(5):665, 2004.

[13] Larry R Baylor, N Commaux, Thomas C Jernigan, NH Brooks, Stephen Kirk Combs, TE Evans, ME Fenstermacher, RC Isler, CJ Lasnier, SJ Meitner, et al. Reduction of edge-localized mode intensity using high-repetition-rate pellet injection in tokamak h-mode plasmas. *Physical review letters*, 110(24):245001, 2013.

[14] RA Moyer, TE Evans, TH Osborne, PR Thomas, M Becoulet, J Harris, K-H Finken, JA Boedo, EJ Doyle, ME Fenstermacher, et al. Edge localized mode control with an edge resonant magnetic perturbation. *Physics of Plasmas (1994-present)*, 12(5):056119, 2005.

[15] W Suttrop, T Eich, JC Fuchs, S Günter, A Janzer, A Herrmann, A Kallenbach, PT Lang, T Lunt, M Maraschek, et al. First observation of edge localized modes mitigation with resonant and nonresonant magnetic perturbations in asdex upgrade. *Physical review letters*, 106(22):225004, 2011.

[16] Bernard Pégourié, Florian Köchl, Hassan Nehme, and Alexei R Polevoi. Recent results on the fuelling and control of plasmas by pellet injection, application to iter. *Plasma Physics and Controlled Fusion*, 51(12):124023, 2009.

[17] PT Lang, A Burckhart, M Bernert, L Casali, R Fischer, O Kardaun, G Kocsis, M Maraschek, A Mlynek, B Plöckl, et al. Elm pacing and high-density operation using pellet injection in the asdex upgrade all-metal-wall tokamak. *Nuclear Fusion*, 54(8):083009, 2014.

[18] G Kocsis, S Kálvin, PT Lang, M Maraschek, J Neuhauser, W Schneider, T Szepesi, et al. Spatio-temporal investigations on the triggering of pellet induced elms. *Nuclear Fusion*, 47(9):1166, 2007.

[19] G Kocsis, JA Alonso, B Alper, G Arnoux, J Figueiredo, D Frigione, L Garzotti, M Lampert, PT Lang, G Petravich, et al. Comparison of the onset of pellet triggered and spontaneous elms. *P-4.136*, 2010.

[20] Peter Thomas Lang, A Alonso, B Alper, E Belonohy, A Boboc, S Devaux, T Eich, D Frigione, K Gál, L Garzotti, et al. Elm pacing investigations at jet with the new pellet launcher. *Nuclear Fusion*, 51(3):033010, 2011.

[21] GTA Huysmans, S Pamela, E Van der Plas, and P Ramet. Non-linear mhd simulations of edge localized modes (elms). *Plasma Physics and Controlled Fusion*, 51(12):124012, 2009.

[22] S Futatani, G Huijsmans, A Loarte, LR Baylor, N Commaux, TC Jernigan, ME Fenstermacher, C Lasnier, TH Osborne, and B Pegourié. Non-linear mhd modelling of elm triggering by pellet injection in diii-d and implications for iter. *Nuclear Fusion*, 54(7):073008, 2014.

[23] RD Durst, WL Rowan, ME Austin, RA Collins, RF Gandy, PE Phillips, and B Richards. Experimental observations of the dynamics of pellet ablation on the texas experimental tokamak (text). *Nuclear fusion*, 30(1):3, 1990.

[24] GA Wurden, K Büchl, J Hofmann, R Lang, R Loch, A Rudyj, and W Sandmann. Pellet imaging techniques in the asdex tokamak. *Review of scientific instruments*, 61(11):3604–3608, 1990.

[25] PB Parks. Theory of pellet cloud oscillation striations. *Plasma physics and controlled fusion*, 38(4):571, 1996.

[26] HW Müller, PT Lang, K Buechl, M Kaufmann, BV Kuteev, PJ McCarthy, V Mertens, I Miroshnikov, W Schneider, H Zohm, et al. Improvement of q-profile measurement by fast observation of pellet ablation at asdex upgrade. *Review of scientific instruments*, 68(11):4051–4060, 1997.

[27] HW Müller, K Büchl, M Kaufmann, PT Lang, RS Lang, A Lorenz, M Maraschek, V Mertens, J Neuhauser, and ASDEX Upgrade Team. High-β plasmoid drift during pellet injection into tokamaks. *Physical Review Letters*, 83(11):2199, 1999.

[28] G Kocsis, L Barrera, JE Boom, T Craciunescu, G Cseh, PT Lang, NC Luhmann Jr., G Náfrádi, HK Park, T Szepesi, and ASDEX Upgrade Team. Investigating pellet ablation dynamics at asdex upgrade. *European Conference Abstracts*, 36F, 2012.

[29] MNA Beurskens, J Schweinzer, C Angioni, A Burckhart, CD Challis, I Chapman, R Fischer, J Flanagan, Lorenzo Frassinetti, C Giroud, et al. The effect of a metal wall on confinement in jet and asdex upgrade. *Plasma Physics and Controlled Fusion*, 55(12):124043, 2013.

[30] PT Lang, P Cierpka, O Gehre, M Reich, C Wittmann, ASDEX Upgrade Team, A Lorenz, D Frigione, S Kalvin, G Kocsis, et al. A system for cryogenic hydrogen pellet high speed inboard launch into a fusion device via guiding tube transfer. *Review of scientific instruments*, 74(9):3974–3983, 2003.

[31] G Kocsis, S Kálvin, G Veres, P Cierpka, PT Lang, J Neuhauser, C Wittman, and ASDEX Upgrade Team. A fast framing camera system for observation of acceleration and ablation of cryogenic hydrogen pellet in asdex upgrade plasmas. *Review of scientific instruments*, 75(11):4754–4762, 2004.

[32] T Szepesi, S Kálvin, G Kocsis, PT Lang, I Senichenkov, and ASDEX Upgrade Team. Comparison of pellet acceleration model results to experimentally observed penetration depths. *Journal of Nuclear Materials*, 390:507–510, 2009.

[33] S Kálvin, G Kocsis, G Veres, and D Wágner. Quasi two-dimensional simulation of the hydrogenic pellet ablation and plasmoid expansion. 2008.

[34] G Veres and LL Lengyel. A collisional–radiative cooling model for light impurity elements in hot plasmas under non-equilibrium conditions. *Journal of nuclear materials*, 250(2):96–102, 1997.

[35] T Feher. Interaction of carbon-doped pellets and hot plasmas. Master's thesis, Eotvos Lorand University, Budapest, Hungary, 2008.